

BASIC PARAMETER ESTIMATION OF BINARY NEUTRON STAR SYSTEMS BY THE ADVANCED LIGO/VIRGO NETWORK

CARL L. RODRIGUEZ¹, BENJAMIN FARR¹, VIVIEN RAYMOND^{1,2}, WILL M. FARR¹, TYSON LITTENBERG¹, DIEGO FAZI¹, VICKY KALOGERA¹

Draft version May 21, 2013

ABSTRACT

Within the next 5 years, the Advanced LIGO/VIRGO network will have reached a sensitivity sufficient to enable the routine detection of gravitational waves. Beyond the initial detection, the scientific promise of these instruments relies on the efficiency of the parameter estimation techniques being currently developed. The majority of this effort has been towards the detection and characterization of gravitational waves from compact binary coalescence, i.e. the coalescence of black holes and/or neutron stars. While several previous studies have focused on the parameter estimation abilities of advanced detectors, the vast majority have relied on approximation techniques (such as the Fisher Matrix) when characterizing the uncertainties. Here, we report the statistical uncertainties that will be achievable, in practice, using the parameter estimation code **LALInference** to recover the parameters of binary neutron star systems detected in various configurations of the Advanced LIGO/VIRGO network. We find that the recovery of the individual masses will be, on average, sufficient to differentiate neutron stars from black holes by the masses alone. We also report the average uncertainties on the sky-locations, luminosity distance, and orbital inclinations of randomly generated sources that can be recovered by the expected three and four-detector networks.

1. INTRODUCTION

By 2016, the field of gravitational-wave astrophysics will mature into an ideal tool for exploring the gravitational side of the universe. Within the next few years, the first generation of gravitational-wave detectors capable of regularly resolving astrophysical sources will come online [CITE]. The Advanced LIGO and VIRGO detectors will provide the first insights into the final moment of binary compact object mergers, including the merger of binary neutron star systems. Intense work is being undertaken to prepare to characterize and extract as much physical information as possible from these signals.

The mergers of binary neutron stars are expected to be the most ubiquitous source in the advanced detector era [CITE]. Models from stellar evolution suggest that the number of binary neutron star mergers within Advanced LIGO/VIRGO's detection horizon could reach into the hundreds per year [CITE]. Although the peak sensitivity of ground-based detectors is not focused on the frequency at which BNS systems merge, it should still be possible to extract information about both strong field gravitational physics [CITE] and the hydrodynamics of dense matter (e.g. the equation of state of nuclear matter) [CITE]. Furthermore, the observations of multiple BNS systems will provide key insight into the evolution of binary systems in the field [CITE], and in globular clusters [CITE]. As such, BNS systems will likely form the “bread and butter” of the compact object efforts in the coming years.

Of course one must distinguish between the detection

of such events, and the precision measurement of the relevant physical parameters. The detection of BNS systems will be performed with a matched filtering approach. By comparing the data stream with a bank of theoretical templates, the roughly 16KHz time-series data can be searched for candidate signals at a sufficiently rapid rate to analyze months of data. When the overlap between one of the template waveforms and the detector output is sufficiently large (97%), a detection candidate is found. However, the parameter space of these signals can be highly degenerate, with several locations in parameter space corresponding to nearly identical waveforms. In order to fully realize the science potential of these instruments, we must perform a full exploration of the parameter space for each detection. By analyzing the parameter space of each candidate with a Bayesian inference technique and proper sampling, we will be able to make precise, scientifically meaningful statements about the physics of these detectible systems. To that end, we employ a Markov-Chain Monte Carlo sampling algorithm, **lalinference_mcmc**, included in the LIGO Application Library parameter estimation code, **LALInference**.

By employing the full parameter-estimation machinery that will eventually be used in the Advanced LIGO/VIRGO era, our results give the first estimate at the realistic capabilities of advanced ground-based detectors to characterize BNS systems. Until recently, the majority of studies have employed the Fisher matrix formalism which was first adapted for gravitational-wave parameter estimation by (Finn 1992). While each of these studies (Poisson & Will (1995); Cutler & Flanagan (1994); Arun et al. (2005), among many others) have pointed out the limitations and flaws of the Fisher Information Matrix, there has been no study which investigates the BNS parameter estimation capabilities of Advanced LIGO/VIRGO via the techniques that will even-

¹ Center for Interdisciplinary Exploration and Research in Astrophysics (CIERA) & Dept. of Physics and Astronomy, Northwestern University, 2145 Sheridan Rd, Evanston, IL 60208, USA; [e-mail: cr@u.northwestern.edu]

² California Institute of Technology, Pasadena, CA 92215, USA

tually be employed. The recent work of Vallisneri (2008) and our own work (Rodriguez et al. 2013) has demonstrated that the Fisher matrix cannot even be treated as a lower bound on the standard deviations of certain parameters (particularly the masses) measurable in gravitational-wave detectors.

In this paper, we perform a systematic study of the statistical uncertainties with which the Advanced LIGO/VIRGO network will be able to measure the basic parameters of binary neutron stars. In Section 2, we describe the machinery of our parameter estimation code, **LALInference**, and the associated MCMC sampler, `lalinference_mcmc`, as well as the frequency-domain gravitational-wave template we employ. In Section 3, we qualitatively analyze the posterior probability density functions for BNS systems with different masses and extrinsic parameters. The results are divided into three parameter sets of interest: the recovery of the mass parameters (Section 3.1), the recovery of the orbital inclination and luminosity distance (Section 3.2), and the isolation of sources in the sky (Section 3.3). Finally we provide quantitative 1-dimensional confidence intervals on the parameter recovery in Section 4. We assume that $G = c = 1$ throughout.

2. PARAMETER ESTIMATION

We begin by introducing a Bayesian formalism for parameter estimation. We assume that the time-domain signal in a gravitational-wave network can be written as a combination of a gravitational waveform h_0 and the noise of the detector n . We further assume that this noise is stationary and Gaussian with mean zero. Therefore, the detector output is simply

$$s = n + h_0. \quad (1)$$

Since our noise model is Gaussian, we can write the probability of a specific signal realization s as proportional to the probability that our signal is Gaussian once the waveform has been subtracted

$$\begin{aligned} p(s|\theta) &\propto \exp \left[-\frac{1}{2} \langle n|n \rangle \right] \\ &= \exp \left[-\frac{1}{2} \langle s - h(\theta) | s - h(\theta) \rangle \right], \end{aligned} \quad (2)$$

where θ is the set of parameters for our template waveforms. The inner product, $\langle | \rangle$, is defined using the noise spectrum of the detectors as

$$\langle a|b \rangle \equiv 4\Re \int \frac{\tilde{a}(f)\tilde{b}^*(f)}{S_n(f)} df, \quad (3)$$

where $S_n(f)$ is the one-sided power spectral density as a function of frequency, and $\tilde{a}(f)$ and $\tilde{b}(f)$ are the Fourier transforms of the time-domain signals $a(t)$ and $b(t)$.

Once we have the likelihood of the signal (2), we employ Bayes Rule to obtain the posterior probability of the system parameters θ given the signal s as

$$\begin{aligned} p(\theta|s) &= \frac{p(\theta)p(s|\theta)}{p(s)} \\ &\propto p(\theta) \exp \left[-\frac{1}{2} \langle s - h(\theta) | s - h(\theta) \rangle \right], \end{aligned} \quad (4)$$

where $p(\theta)$ are the prior probabilities on our source parameters and $p(s)$ is a normalization constant. Our prior information can come from physics limits in the parameter space, or from our *a priori* knowledge of astrophysical systems. If we pick a set of parameters θ such that $h(\theta) = h_0$, then the posterior (4) will be near a global maximum; however, the presence of noise will in general deflect the maximum of our posterior away from the value at θ_0 . That is, in the presence of noise, there is no guarantee that the maximum-likelihood of our signal corresponds to the true parameters of the system.

2.1. Markov-Chain Monte Carlo

The LIGO Algorithm Library parameter estimation code, **LALInference**, is designed as a unified framework for gravitational-wave parameter estimation. By using a common setup for waveform generation, PSD estimation, data handling, and other associated techniques from gravitational-wave parameter estimation, **LALInference** allows the implementation of multiple parameter samplers in using identical parameter setups, including nested sampling (`lalinference_nest`) and Markov-Chain Monte Carlo (`lalinference_mcmc`). We elect to use the MCMC sampler for this study. `lalinference_mcmc` is based upon the previously described code, **SpinSpiral** (van der Sluis et al. 2009; Raymond et al. 2010). The MCMC employs a Metropolis-Hastings sampling algorithm, which can be described as follows (Gilks 1999):

1. Pick an initial point in the parameter space (θ_{old}), and then propose a random “jump” to a new set of waveform parameters, θ_{new} . The jump follows the (conditional) probability distribution $q(\theta_{\text{new}}|\theta_{\text{old}})$.
2. Calculate the posterior probability, $p(\theta_{\text{new}}|s)$, of the new parameters using (2) and (4).
3. Accept the new parameters with probability

$$p_{\text{accept}} = \min \left[1, \frac{p(\theta_{\text{new}}|s)q(\theta_{\text{old}}|\theta_{\text{new}})}{p(\theta_{\text{old}}|s)q(\theta_{\text{new}}|\theta_{\text{old}})} \right]. \quad (5)$$

If the new parameters are accepted, record θ_{new} and repeat with $\theta_{\text{old}} \leftarrow \theta_{\text{new}}$; otherwise, record θ_{old} , and repeat.

The above procedure is designed to record a chain of samples whose distribution is $p(\theta|s)$. Depending on the proposal distribution, q , the convergence (mixing) of the chain may be rapid or slow. We employ multiple optimization techniques, including both specially-crafted q and parallel tempering, to ensure adequate mixing of the Markov Chains throughout our parameter space. The details of the algorithm can be found in (van der Sluis et al. 2008, 2009; Raymond et al. 2010). Both samplers were tuned and developed during the last science run of the Initial LIGO/VIRGO network. A description of the parameter estimation capabilities, c.f. 2010, can be found in the LIGO Scientific Collaboration et al. (2013).

2.2. Waveform Model

We use a frequency domain waveform accurate up to 3.5 post-Newtonian (pN) order in phase and amplitude. We restrict ourselves to quasi-circular waveforms as a

simplifying assumption. The standard form of our waveform model, known as the *TaylorF2* approximant, is calculated via the stationary-phase approximation. In this setup, the gravitational-wave amplitude is given by

$$\tilde{h}(f) = Af^{-7/6}e^{i\psi(f)}, \quad (6)$$

where $A \propto \mathcal{M}_c^{5/6}\Theta(\text{angle})/D$, D is the luminosity distance of the binary, and $\psi(f)$ is the pN phase. $\Theta(\text{angle})$ is a function of the orbital orientation with respect to the detector network in terms of the sky position, orbital inclination, and the wave polarization. In addition to the total mass, $M \equiv M_1 + M_2$, it is convenient to work with the *mass ratio* and *chirp mass*, defined by

$$q \equiv M_1/M_2 \quad \text{and} \quad \mathcal{M}_c = (M_1 M_2)^{3/5} M^{-1/5}, \quad (7)$$

respectively.³ The stationary phase then becomes an expansion in the Newtonian orbital velocity, $v = (\pi M f)^{1/3}$,

$$\psi(f) = 2\pi f t_c - \phi_0 + \frac{\pi}{4} + \frac{3}{128} \left(\frac{M}{\mathcal{M}_c} \right)^{5/3} \sum_{k=0}^n \alpha_k v^{k-5} \quad (8)$$

where the α_k coefficients are taken from the pN expansion to order $n/2$. See Buonanno et al. (2009) for a description and comparison of different waveform families.

The terms t_c and ϕ_0 in equation (8) are constants of integration, referred to as the chirp time and coalescence phase, respectively. Although uninteresting physically, they must be accounted for in any parameter estimation study of the waveform phase.

To perform the integral defined in (3), we used as our power-spectral density the best estimate for a high-power, zero-detuning configuration of Advanced LIGO, provided by the LIGO Scientific Collaboration. Both the noise curve and technical reports describing it can be found in Shoemaker (2009). We consider two configurations of the advanced detector network: a three-detector configuration consisting of the two LIGO sites (in Hanford, WA and Livingston, LA) and the Virgo site (in Pisa, Italy), and a four-detector configuration with adds the proposed LIGO-India detector (in Chitradurga, KA). For simplicity, we assume each detector to be operating at the Advanced LIGO sensitivity.

For a multi-detector network, the noise-weighted inner products (3) combine linearly, allowing us to use the above formalism with minimal modification. We integrate the inner product from a lower-frequency cutoff of 20Hz to the innermost-stable-circular orbit of the systems in question, which for a non-spinning binary is a function only of the total mass:

$$\pi f_{\text{ISCO}} = \frac{1}{6^{3/2} M}. \quad (9)$$

We consider the mass parameters (\mathcal{M}_c, q) and the phasing parameters, (ϕ_0, t_c) , to be the intrinsic parameters of a gravitational-wave signal. There are an additional 5 extrinsic parameters, independent of the pN orbital phase, which can modulate the amplitude of the signal

³ Most gravitational-wave literature instead uses the *symmetric mass ratio*, defined as $\eta \equiv M_1 M_2 / M^2$. We elect to use q as it is empirically superior when proposing MCMC parameter jumps, and is more physically intuitive.

in an independent fashion for each detector. Combining these leads to our 9-dimensional parameter space for non-spinning systems:

$$\theta = (\mathcal{M}_c, q, \phi_0, t_c, D, \iota, \psi, \alpha, \delta) \quad (10)$$

where to summarize

- \mathcal{M}_c is the chirp mass,
- q is the mass ratio,
- ϕ_0 and t_c are the chirp phase and chirp time, arbitrary phasing parameters,
- D is the luminosity distance to the binary,
- ι is the orbital inclination,
- ψ the gravitational-wave polarization, and
- α and δ the right ascension and declination of the source on the sky.

Since the wave amplitude depends on the orientation of the binary with respect to each detector, most of the information about these extrinsic parameters comes from two sources: the time-of-arrival triangulation of the source locations, and the relative amplitudes within the detector network.

We define the signal-to-noise ratio (SNR) of a gravitational wave in a single detector as

$$\rho \equiv \frac{4}{\sigma} \int_0^\infty \frac{|\tilde{s}(f)\tilde{h}^*(f)|}{S_n(f)} df \quad (11)$$

where ρ is the SNR and $\tilde{s}(f)$ and $\tilde{h}^*(f)$ are the frequency-domain signal and template, respectively, and the normalization σ is given by

$$\sigma^2 = 4 \int_0^\infty \frac{|\tilde{h}(f)|^2}{S_n(f)} df. \quad (12)$$

When dealing with network of gravitational-wave detectors, the SNRs of the individual detectors add in quadrature. That is, the network SNR for a detection is

$$\rho_{\text{network}} = \sqrt{\sum_i \rho_i^2} \quad (13)$$

where ρ_i is the SNR, given by (11), of the i^{th} detector.

For this study, we consider four separate populations of BNS systems, with component mass combinations of $1M_\odot/1M_\odot$, $1.4M_\odot/1.4M_\odot$, $1M_\odot/2.5M_\odot$, and $2.5M_\odot/2.5M_\odot$. Each population consisted of 40 signals distributed randomly in sky location, polarization, inclination, time-of-arrival, and coalescence phase. The luminosity distance, D , was selected to provide a network SNR of $\rho_{\text{network}} = 20$ for each source. While unphysical from an astrophysical perspective (binary sources should be distributed evenly in comoving volume), this choice allows us to explore the parameter estimation in the context of viable detection candidates.

Finally, note that the power-spectral density that defines the inner product (3) is simply the time-averaged

sensitivity of a given detector to a specific frequency. Ignoring non-Gaussian glitches, any stretch of data should contain a specific noise realization drawn from a Gaussian colored by the PSD. However, what we are interested in is not the parameter estimation that can occur in a specific draw from this probability of noises, but the uncertainties averaged over all possible noise realizations.⁴ Since our noise model is assumed to be Gaussian, it is unnecessary to recover the parameters from a large sample of identical waveforms in different noise; we can simply assume the noise is the mean defined by the power-spectral density. This “zero-noise” parameter estimation provides a statical statement on the measurable uncertainties, and is what is reported here. In Section 3.5 we provide an example of parameter estimation in several non-zero noise realizations compared to the zero-noise equivalent.

3. RESULTS

Of the 9 parameters in the domain of the waveform, only 6 are particularly physically interesting: the masses of the two binaries, M_1 and M_2 , the orbital inclination, ι , the angular position on the sky, α and δ , and the luminosity distance of the source, D . While the coalescence phase ϕ_c , the coalescence time t_c , and the wave polarization ψ must be included in any parameter estimation of the waveform, they do not encode any information of particular astrophysical interest.⁵

In Figure 1, we provide an example of the 9, 1-dimensional marginalized posterior probability density functions recovered from a single $1.4M_\odot/1.4M_\odot$ BNS system. These PDFs are typical of what will be produced by parameter estimation studies in the advanced detector era. Notice that the peak of several parameters, including the chirp mass, \mathcal{M}_c , appears to be displaced from the true values in red. This effect is due to the reduction of the 9-dimensional PDF to a series of marginalized 1-dimensional PDFs. For instance, the 1-dimensional PDF for chirp mass is marginalized via

$$p(\mathcal{M}_c|s) = \int_{\theta \setminus \mathcal{M}_c} p(\theta|s) d(\theta \setminus \mathcal{M}_c) \quad (14)$$

where the notation $\theta \setminus \mathcal{M}_c$ implies all parameter of (10) except \mathcal{M}_c . Other parameter and higher-dimensional marginalizations follow a similar convention.

3.1. Mass Parameters

Of the 9 variables in our parameter space (10), the two of immediate physical interest are the two parameters, \mathcal{M}_c and q , or correspondingly the direct masses of the two companions, M_1 and M_2 . As stated above, the ability of Advanced LIGO/VIRGO to construct a population of BNS masses will be critical to the science potential of gravitational-wave astronomy.

We find that there is virtually no difference between the mass PDFs of our different injected signals within each mass bin. While this may initially seem disconcerting, it is to be expected. Recall that of the BNS signals

were injected with a network SNR of 20 into a zero-noise detector realization. Furthermore, note that the mass parameters are the only two which directly effect the phase of the TaylorF2 waveform (8). Therefore, as long as the injected mass parameters are identical within each mass system, and as long as the injected SNR is identical, the amount of recoverable information in each mass parameter should be almost identical, and for a sufficiently converged MCMC chain, the recovered posterior PDF should be almost identical.

The “almost” in the previous sentence is to draw attention to one critical, neglected fact: while the mass parameters are independent of the injected signals position with respect to the detector network, the other parameters are certainly not. Obviously many of the other parameters (i.e. sky location, polarization, distance, inclination, and time-of-arrival) all depend on the orientation of the binary with respect to each of the individual detectors. Since our 9-dimensional parameter space can be highly correlated, it is entirely reasonable to assume that cross-correlations between the extrinsic parameters and the mass parameters will cause variation in the recovery of the individual injection PDFs.

In practice, it was found that the cross-correlations between the extrinsic parameters and signal time-of-arrival were several orders of magnitude [QUANTIFY] below the uncertainties in \mathcal{M}_c and q . It should be noted that, in practice, this will not be the case: in reality, the noise power-spectral density of each detector varies as a function of time, including both natural variations in sensitivity and detector glitches [CITE]. In such a case, the base sensitivity of a gravitational-wave detector to even the easiest to recover parameters will vary as a function of position and time.

In Figures 2 and 3, we show the marginalized 2D posterior PDFs of our mass parameters a prototypical equal mass and unequal mass binaries. We include the PDF in both the \mathcal{M}_c - q space (relevant for the waveform and the MCMC algorithm), and the more physically interesting component mass space (M_1 - M_2). Although only the $1.4M_\odot/1.4M_\odot$ system is included in Figure 2, the PDF is virtually identical to the other equal mass cases, modulo a scaling factor. Again, this is unsurprising due to the identical SNR of each of the injected signals.

As the PDFs of the masses are virtually identical, we average the 1-dimensional mass PDFs into a single posterior probability for system. See Figure 4. Notice how when averaged and normalized to the injected values, the recovery of the component masses depends only on the mass ratio. Furthermore, for systems of equal masses, the posterior barely extends beyond 15% of the injected values (see also Table 1 in Section 4). If one assumes that the threshold between black holes and neutron stars lies at approximately $3M_\odot$ [CITE WILL], then it will be possible to reliably distinguish the components of each inspiral as a neutron star.

3.2. Inclination and Distance

Since it is assumed that binary neutron star systems (along with neutron star/black hole systems) are the progenitors for short gamma-ray bursts, emitting the burst along the axis of orbital angular momentum, the inclination of the binary system will be of particular interest to gamma-ray astronomy [CITE]. The inclination is de-

⁴ Similarly to how the Fisher matrix formalism can provide the Cramer-Rao bound averaged over all noise realizations

⁵ For systems whose components are non-spinning. The presence of intrinsic angular momentum will, in general, couple to the coalescence phase and wave polarization.

Example 1D Posterior Probability Densities for $1.4M_{\odot}/1.4M_{\odot}$ System

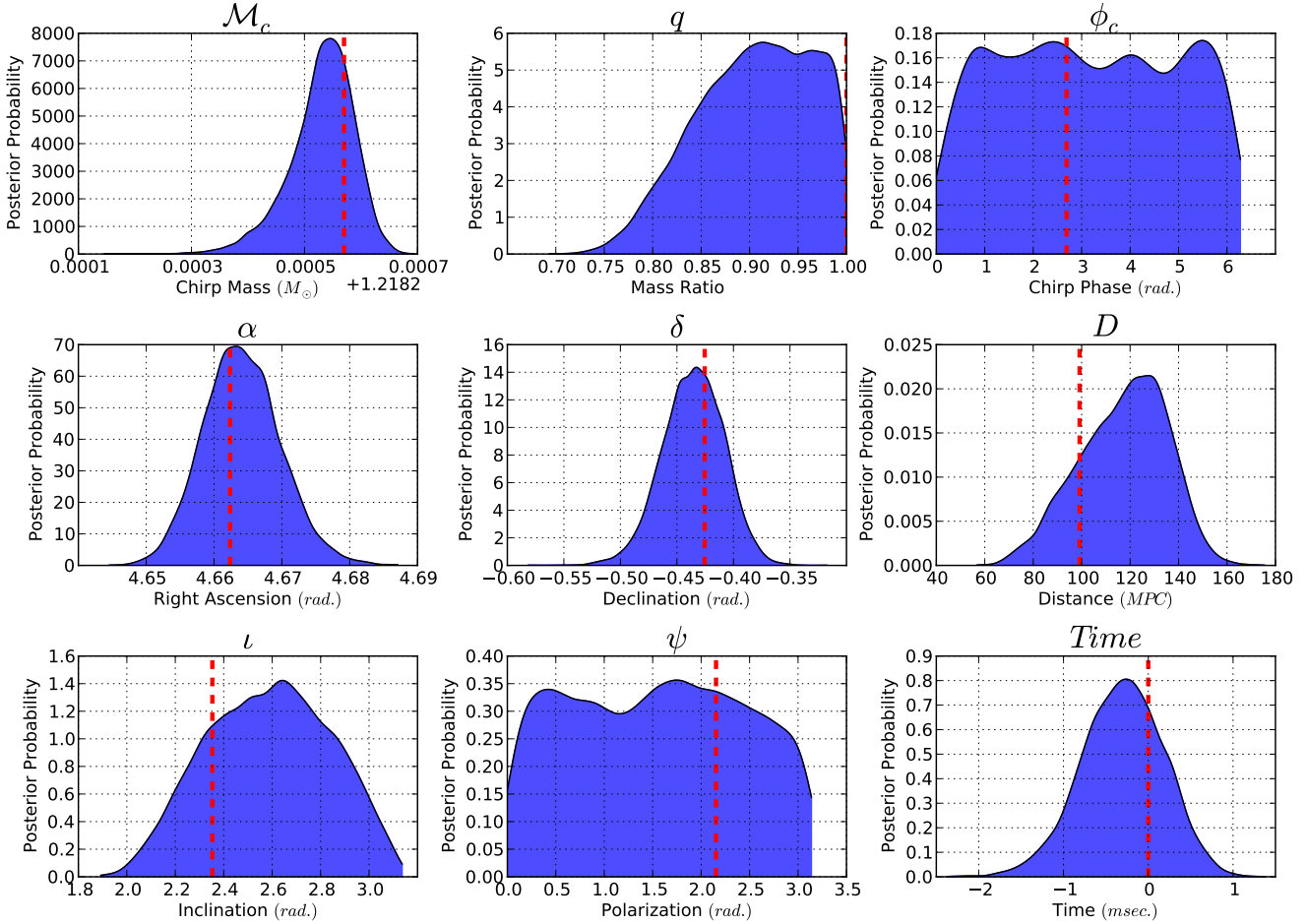


FIG. 1.— Marginalized 1D posterior probability density functions taken from a typical $1.4M_{\odot}/1.4M_{\odot}$ BNS system. We have plotted each of the 9 parameters for our non-spinning BNS problem as stated in section 2.2. Note how, even for parameters with excellent recovery, the peak of the 1D Gaussian is displaced from the injected value (in dashed red). This is not due to a systematic bias, but is caused by the marginalization of a single dimension from the full 9D posterior space. To better see this effect, compare the 1D PDF for M_c and q with the 2D marginalized PDF in Figure

tected as a relative amplitude difference between the two gravitational-wave polarization, such that to lowest order

$$\begin{aligned} h_+(f) &= \frac{1 + \cos^2(\iota)}{2D} \tilde{h}(f) \\ h_{\times}(f) &= i \frac{\cos(\iota)}{D} \tilde{h}(f) \end{aligned} \quad (15)$$

It should be apparent that the luminosity distance D and the inclination ι can be highly correlated in any parameter estimation study, given that both terms modulate the amplitude of a gravitational wave [QUANTIFY THIS],

Given this degeneracy, it should come as no surprise that the 2D marginalized posteriors of distance and inclination are the worst of the 6 parameters of physical interest. Four typical 2D PDFs are presented in Figure 5. Notice the large, bimodal uncertainties present in some of the 2D PDFs along the ι axis, due to the similarity between the evaluated likelihoods at ι and $\iota + \pi/2$. As the majority of the information extracted via param-

eter estimation is from the phase of the signal, the recovery of a posterior in D - ι space will be limited, even during the Advanced LIGO/VIRGO era; however, there will be cases (such as the first PDF in Figure 5) that will prove copacetic to simultaneous measurements accurate enough for coincidence measurements with GRB observers.

3.3. Sky Localization

Unlike the mass parameters, the recovery of the position on the sky is highly dependent on the location of the source with respect to the detector network in question. For the HLV configuration, the three-detector network can only localize signals to one of two points in the sky. That is, when using only time-of-arrival information, there is equal support in the probability density functions at the true location and at the point reflected through the plane formed by the three detectors. In practice, correlated information from the wave polarization can break this degeneracy, so for runs in zero noise, the

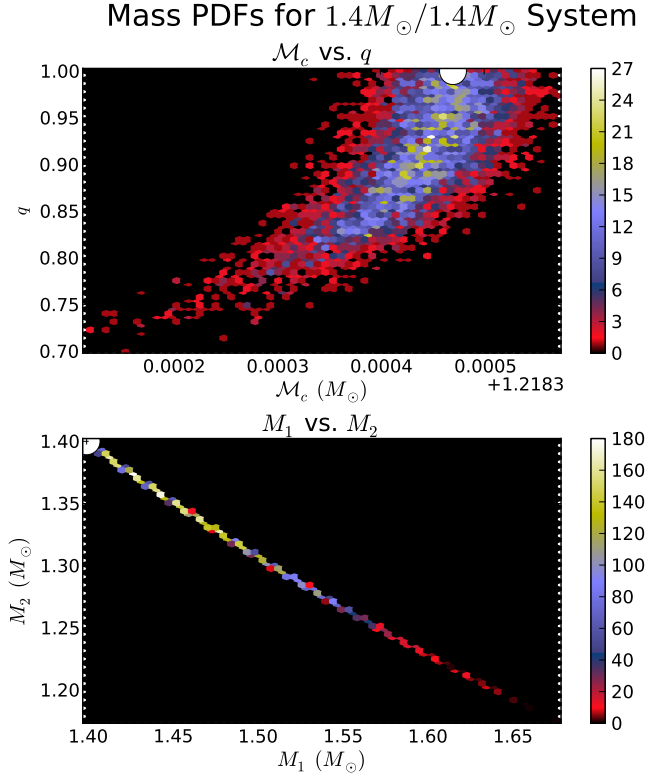


FIG. 2.— 2D marginalized posterior probability density functions for the mass parameters recovered in typical a $1.4M_{\odot}/1.4M_{\odot}$ system. The posteriors are plotted in terms of parameters used in the waveform, chirp mass (M_c) and the mass ratio (q), and in the individual component masses of the binary (M_1 and M_2). In the M_c - q space, the posterior would resemble a Gaussian if not for the limitation of $q \leq 1$. The presence of the q cutoff and the convention that $M_1 \geq M_2$ inform the non-Gaussian features present. When projected as 1D marginalized posteriors, the component masses resemble the posterior PDFs shown in figure 4.

MCMC properly explores the correct peak on the sky.

The sky location uncertainties for HLV and HLVI are shown in Figures 6 and 7 respectively. We show all four mass bins together, since in practice the mass of the signals had no effect on the recovery of the sky location. Only the location on the sky, the network configuration, and the other extrinsic parameters were found to be relevant. In particular, notice the increase in efficiency between the HLV configuration and the HLVI configuration. This is hardly surprising, since four detectors allows one to accurately isolate any signal using time-of-arrival. In the case of the three-detector configuration, there exist locations in the sky in which a signal is close to its degeneracy point (the point reflected through the plane of the three detectors). The posteriors recovered for signals from these locations tend to appear stretched, achieving posterior support at both points. See [CITE FAIRHURST] for a global analysis of time-of-arrival accuracy for various network configurations, and [LIGO INDIA PAPER]

3.4. Testing MCMC Convergence

Each set of MCMC samples is tested for convergence by examining both the Gelman-Rubin diagnostic and the auto-correlation length of the MCMC chains, the details of which can be found in [CITE] and [CITE], respec-

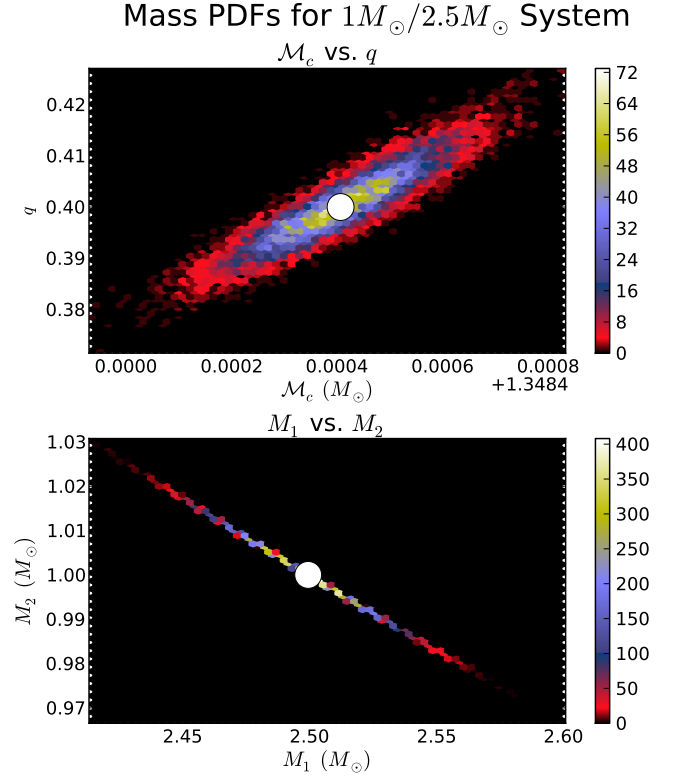


FIG. 3.— Similar to Figure 2, for a typical $1M_{\odot}/2.5M_{\odot}$ system. The unequal mass ratio displaces the posterior PDFs from the $q \leq 1$ present in the equal mass case, yielding a Gaussian PDF in both the M_c - q and M_1 - M_2 spaces.

tively. However, there is an additional check we can consider: the standard matched filtering searches employed by the LIGO/VIRGO collaboration assume that a detection will occur when one of the template waveforms matches the detector data with a signal overlap of 97% or better [CITE]. That is, for a template waveform $h^t(f)$ and detector output $s(f)$, an overlap of

$$\langle s|h^t \rangle \geq 97\%$$

yields a detection candidate. This requirement provides us with a convenient test for the effectiveness of our parameter estimation. First, we note that maximizing our likelihood function, (2), is identical to maximizing the SNR (11) of our template waveform in a given stretch of data. Therefore, the better the match between the template waveform and the data, the higher the SNR. Since we assume, quite tautologically, that our parameter estimation code should estimate parameters at least as well as a matched filtering approach, we would be immediately suspicious of any MCMC run whose maximum-likelihood waveform had an SNR below that of our pipeline trigger. In that case, we would perform the MCMC with a much longer runtime, until the maximum likelihood of our posterior distribution had an SNR at least as high as the detection.

For the purposes of our present study, we reproduce this information as follows: since we know the true SNR of the signal we are simulating, we assume that the “trigger” SNR returned by our detection pipeline is 97% of the true SNR. We then assume any posterior distribution

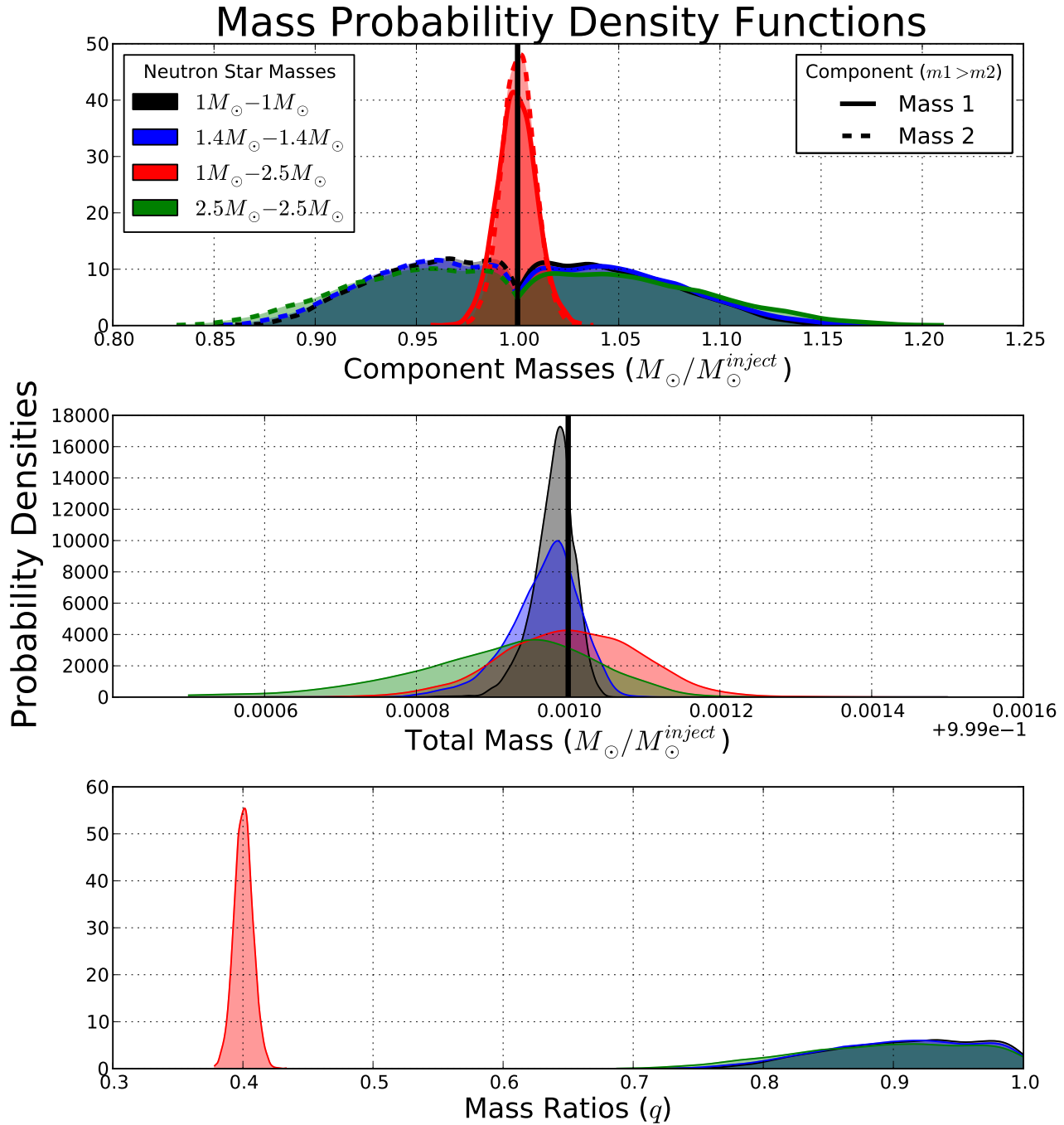


FIG. 4.— Mass PDFs for the four BNS systems, averaged over each of the 40 injections. The average is reported since, in practice, there was virtually no difference between the recovered PDFs for different systems with identical masses and SNRs [QUANTIFY]. Notice how the PDFs for systems with identical mass ratios but different total masses are identical when normalized to the true total mass.

whose maximum likelihood satisfies

$$\text{Maximum Likelihood} \leq 0.97 \times \left(\frac{\rho_{inj}^2}{2} \right)$$

has not converged. As one would expect, the lower-mass, longer waveform systems require longer to converge. With our original runtime of one week over 8 processors, we found that seven of our $1M_{\odot}/1M_{\odot}$ systems had not converged, while all but one system for our $1.4M_{\odot}/1.4M_{\odot}$ and $1M_{\odot}/2.5M_{\odot}$ systems had converged.

All of the $2.5M_{\odot}/2.5M_{\odot}$ systems converged within one week.

[THIS SECTION INCOMPLETE WILL REQUIRE THE FINISHED HLV/HLVI RUNS BEFORE I CAN COMPLETE IT]

3.5. Varied Noise Realizations

While we have, for a variety of reasons, performed the current analysis on zero-noise injections, parameter estimation in the advanced detector error will not be so copacetic. Each detection will occur in noisy data, with a specific realization of the PSD provided and with pos-

Distance/Inclination PDFs

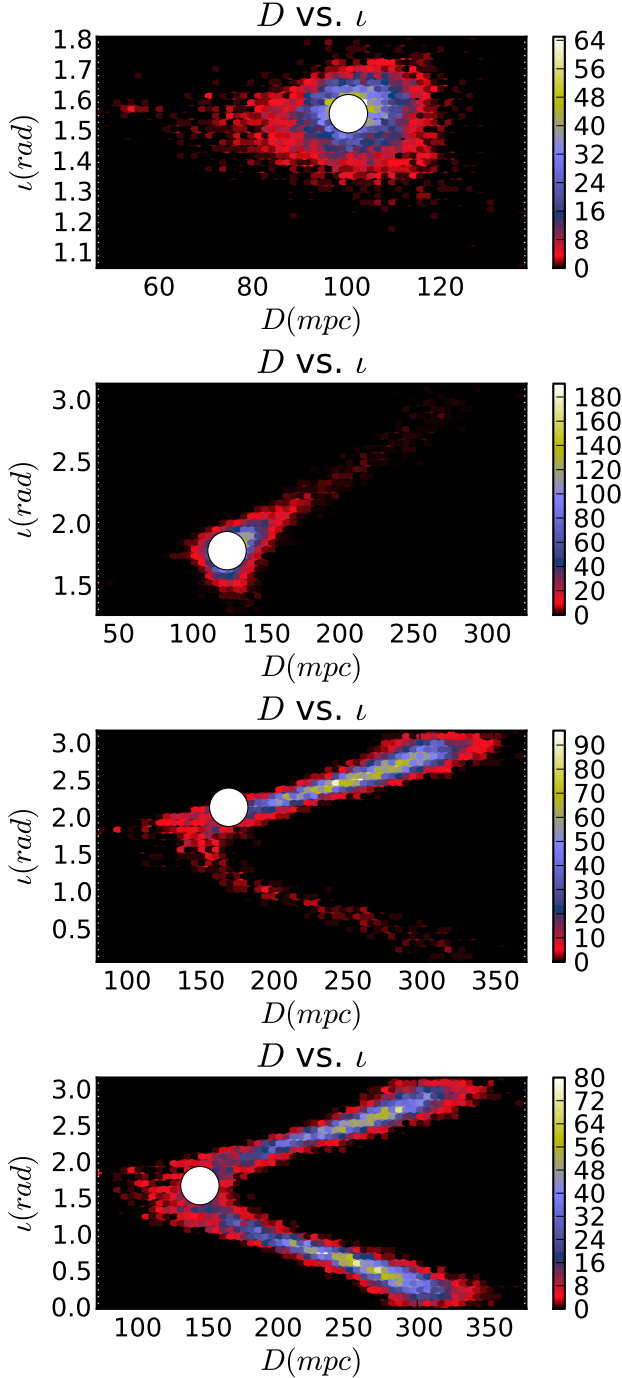


FIG. 5.— Typical marginalized 2D mass PDFs for luminosity distance D and orbital inclination ι .

sible instrumentation and environmental glitches. In the case of a unique Gaussian realization of the Advanced-LIGO noise curve, each realization causes the maximum likelihood of the posterior probability distribution to be translated away from the true value; however, these displacements are drawn according to the zero-noise distri-

bution (Rodriguez et al. 2013). Once averaged, the mean uncertainties should be equal to the uncertainty drawn from the zero-noise runs.

As a demonstration of this, we injected a single $1.4M_{\odot}/1.4M_{\odot}$ system, detected in HLVI, into 5 separate realizations of Gaussian noise colored by the Advanced LIGO PSD, and compared the results to the same MCMC recovery in the zero-noise case. This example can be seen for one-dimensional marginalization of M_c and q in Fig. 8. In effect, the “real answer” that will be recovered is a single PDF with similar width to the zero-noise PDF, but with the peak likelihood displaced from the true value.

Of course, the largest concern for gravitational-wave parameter estimation will not be the specific realization of Gaussian noise, but the effects of glitches in the data. These time-series glitches have a variety of well-known and not-so-well-known physical causes in the instrument, and can cause substantially greater errors in parameter recovery than any specific realization noise realizations. This has already been addressed for the case of space-based gravitational-wave detectors (LISA), and is currently being implemented in `lal inference_mcmc` [CITE TYSON, PROTO-TYSON].

4. CONFIDENCE INTERVALS

The correct answer to the question “how well can Advanced LIGO/VIRGO measure the parameters of binary neutron star systems” is the full 9-dimensional PDFs; however, for both convenience and comparison, it is useful and elucidating to speak in terms of the confidence intervals of a single parameter. To that end, we state the averaged 65% and 90% confidence intervals about the single parameters for each of the three parameter pairs of interest. These were already plotted for the sky locations in Figures 6 and 7.

There are several different ways of computing the width of a confidence interval in this setup. If one considers the points in the MCMC as random draws from the true posterior, then the α -level confidence interval can be computed by simply ordering the points, removing $N(1 - \alpha)/2$ points from both sides of the posterior samples symmetrically, and measuring the width of the remaining points. While this procedure can prove hazardous for multi-modal distributions, it is straightforward and reliable for single-peaked distributions as reported here.

In Table 1, we list the mean 65% confidence intervals recovered for the four mass configurations in both network configurations. This essentially quantifies the widths of the posteriors plotted throughout Section 3. Again, it is worth noting how the small confidence intervals on the individual component masses suggest it will be possible, on average, to discern neutron stars from black holes in binary inspirals. The purpose of Table 1 is to provide a quantitative and quotable source for studies seeking to determine how well a physical question about BNS systems can be answered with the Advanced LIGO/VIRGO network.

5. CONCLUSION

In this paper, we performed an MCMC parameter estimation analysis on the recoverability of basic information about binary neutron stars, using two projected version

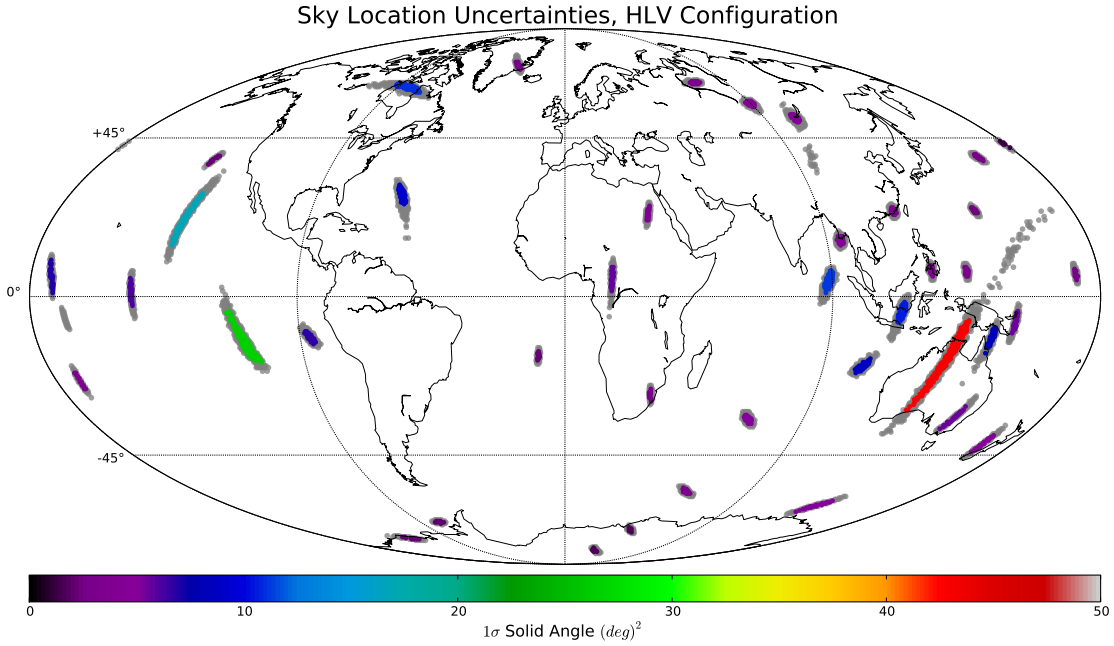


FIG. 6.— The uncertainty on the sky of 160 BNS systems in the HLV detector configuration. Each region represents a single injection, with the colored central region representing the 65% uncertainty region on the sphere, and the gray region representing the 90% uncertainty region. The color scheme indicates the total solid angle size of the 65% region. Note the similar shape of the uncertainty regions at particular points; this is due to the specific realization of our network pattern sensitivity.

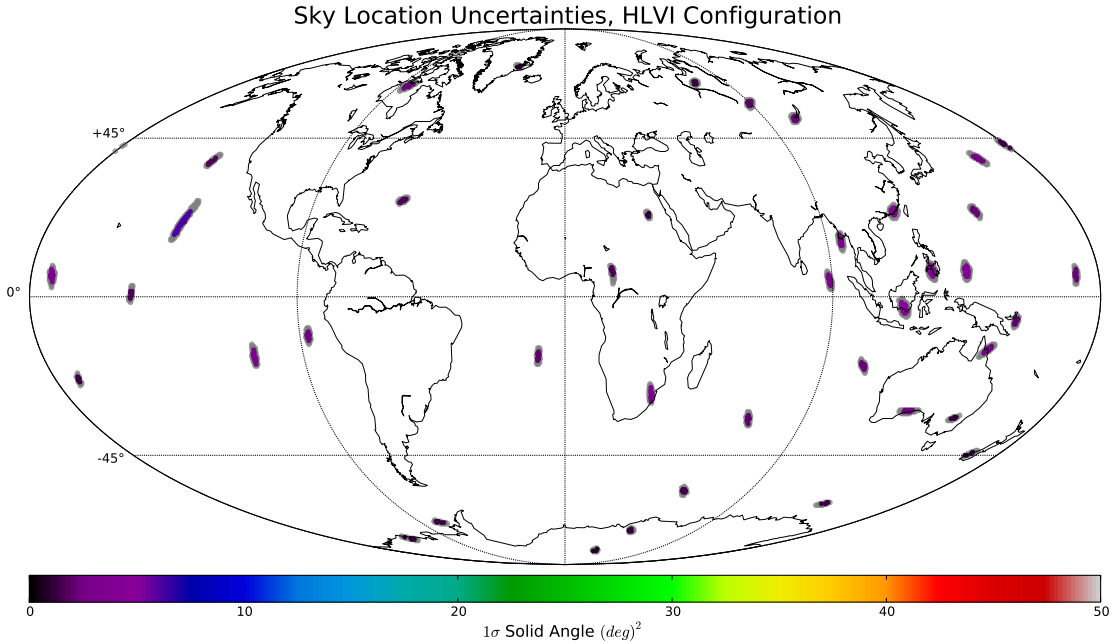


FIG. 7.— The same as Fig 6, except for the HLVI detector configuration. Note the substantially lower average uncertainties on the skies for the majority of the injections. Also note the lack of large, “banana-shaped” uncertainties that were recovered by the HLV configuration. The two improvements are due to the breaking of the degeneracy in sky location recovery that is facilitated by the transition to a four-detector network.

of the Advanced LIGO/VIRGO network. We focused on the recovery of the two masses, the luminosity distance, orbital inclination, and the sky location, as these are the

six basic parameters of physical interest to the problem. We found that [WAIT UNTIL RUNS ARE DONE AND TABLE IS FINISHED TO SUMMARIZE RESULTS]

TABLE 1

65% CONFIDENCE INTERVALS, BUT SINCE THEY'RE INCOMPLETE THESE ARE JUST PLACE HOLDERS FOR NOW (THE REAL ONES WILL HAVE UPPER AND LOWER BOUNDS, AS WELL AS UNITS, NORMALIZATION TO THE INJECTED VALUES, 2D SKY AREAS, AND COMPONENT MASSES) ALSO, DOUBLE CHECK THE RA ON 2.5 2.5 HLVI

HLVI						
System	$\Delta\mathcal{M}_c$	Δq	ΔD	$\Delta\iota$	$\Delta\alpha$	$\Delta\delta$
$1M_\odot - 1M_\odot$	4.33×10^{-5}	0.123	39.1	0.45	0.028	0.028
$1.4M_\odot - 1.4M_\odot$	1.07×10^{-4}	0.13	60.3	0.45	0.028	0.028
$1M_\odot - 2.5M_\odot$	2.37×10^{-4}	0.014	70.13	0.52	0.029	0.030
$2.5M_\odot - 2.5M_\odot$	0.53×10^{-4}	0.15	111.67	0.56	0.18	0.030

HLV						
System	$\Delta\mathcal{M}_c$	Δq	ΔD	$\Delta\iota$	$\Delta\alpha$	$\Delta\delta$
$1M_\odot - 1M_\odot$	4.33×10^{-5}	0.123	46.14	0.55	0.26	0.11
$1.4M_\odot - 1.4M_\odot$	1.08×10^{-4}	0.13	56.3	0.57	0.125	0.130
$1M_\odot - 2.5M_\odot$	2.37×10^{-4}	0.014	66.05	0.66	0.05	0.070
$2.5M_\odot - 2.5M_\odot$	0.53×10^{-4}	0.15	109.5	0.70	0.20	0.06

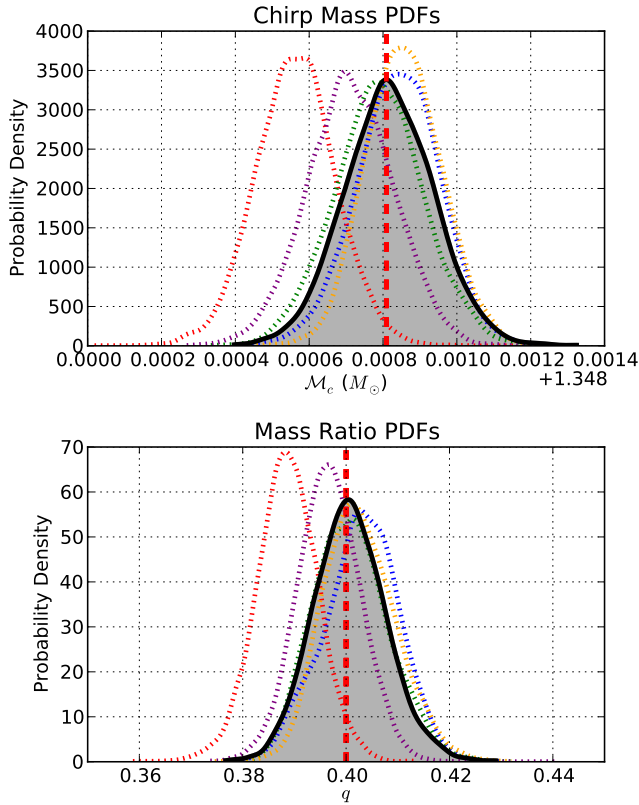


FIG. 8.— The effects of a non-zero noise realization on the recovered PDF for five different Gaussian realizations of the Advanced LIGO noise curve. Each PDF represents the recovery of the same $1M_\odot/2.5M_\odot$ signal in a different noise curve, picked at random from the Gaussian colored noise defined by the Advanced LIGO power spectral density. Notice how the curve is relatively unchanged, but usually assumes a Gaussian PDF displaced from the true value. This only holds true for glitch-free data, which is an unrealistic idealization when compared to real data.

It should be noted that there are two distinct types of systematic error, highly relevant to the gravitational-wave parameter estimation problem, that we have not addressed in this study. First, we have studied the parameter estimation uncertainties under the assumption that the waveform template we use to recover the signal template exactly matches the fully relativistic waveforms nature provides. In practice, these waveforms are only approximations to the fully general-relativistic physics required to solve the problem. See [CITE] for a better description of the systematic uncertainties present in the most common waveform families.

Secondly, as stated above, the noise realization that we have employed here is an substantial idealization. In practice the noise levels of Advanced LIGO and Advanced VIRGO will be highly variable over time, and will not be stationary or Gaussian, as is commonly assumed. Unfortunately, there is no reliable or simple way to simulate the sort of non-Gaussian detector glitches and instrumentation effects that will arise in any advanced gravitational-wave detector. Since the realization of noise will be the primary factor in the deflection of true signal PDFs from the averages quoted here, this effect will be critical to properly characterizing gravitational-wave detections [CITE TYSON AGAIN].

In this study, we have ignored several of the more interesting parameters that can be included in parameter estimation, such as modifications to general relativity [CITE] and the neutron star equation-of-state [CITE]. We elected to focus on the basic parameters that will be measured routinely in the Advanced Detector era. Future work will explore how well these specific questions can be answered using LALInference, and what prospects such parameter estimation will have for answering long-standing questions in relativistic astrophysics.

REFERENCES

- Arun, K. G., Iyer, B. R., Sathyaprakash, B. S., & Sundararajan, P. A. 2005, Phys. Rev. D, 71, 084008, 084008
 Buonanno, A., Iyer, B. R., Ochsner, E., Pan, Y., & Sathyaprakash, B. S. 2009, Phys. Rev. D, 80, 084043, 084043
 Cutler, C., & Flanagan, É. E. 1994, Phys. Rev. D, 49, 2658, 2658
 Finn, L. S. 1992, Phys. Rev. D, 46, 5236, 5236
 Gilks, W. R. 1999, Markov Chain Monte Carlo In Practice
 Poisson, E., & Will, C. M. 1995, Phys. Rev. D, 52, 848, 848

- Raymond, V., van der Sluys, M. V., Mandel, I., et al. 2010, Classical and Quantum Gravity, 27, 114009, 114009
- Rodriguez, C. L., Farr, B., Farr, W., & Mandel, I. 2013, arXiv:Working on it...
- Shoemaker, D. 2009, Advanced LIGO anticipated sensitivity curves
- the LIGO Scientific Collaboration, the Virgo Collaboration, Aasi, J., et al. 2013, ArXiv e-prints, arXiv:1304.1775
- Vallisneri, M. 2008, Phys. Rev. D, 77, 042001, 042001
- van der Sluys, M., Mandel, I., Raymond, V., et al. 2009, Classical and Quantum Gravity, 26, 204010, 204010
- van der Sluys, M. V., Röver, C., Stroer, A., et al. 2008, Astrophys. J. Lett., 688, L61, L61